

GLOS: Sign Language Generation with Temporally Aligned Gloss-Level Conditioning

Taeryung Lee^{1,3} Hyeongjin Nam^{1,2,3} Gyeongsik Moon⁴ Kyoung Mu Lee^{1,2}

¹ IPAI & ASRI, ² Dept. of ECE, Seoul National University, Korea
³ KRAFTON ⁴ Dept. of CSE, Korea University, Korea

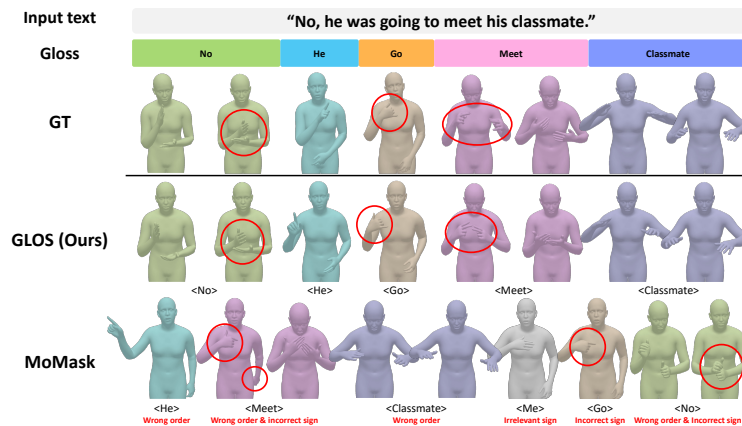


Figure 1: Qualitative comparison between our proposed **GLOS** and prior method (MoMask [12]). We represent the glosses with colors, and the sign segments corresponding to each gloss are painted in the same color. Human-interpreted glosses of generated signs are denoted in brackets $\langle \rangle$ below the signs. While the signs generated by the prior method exhibit incorrect lexical order and include inaccurate signs, our GLOS produces signs in the correct order with accurate movements.

Abstract

Sign language generation (SLG), or text-to-sign generation, bridges the gap between signers and non-signers. Despite recent progress in SLG, existing methods still often suffer from incorrect lexical ordering and low semantic accuracy. This is primarily due to sentence-level condition, which encodes the entire sentence of the input text into a single feature vector as a condition for SLG. This approach fails to capture the temporal structure of sign language and lacks the granularity of word-level semantics, often leading to disordered sign sequences and ambiguous motions. To overcome these limitations, we propose **GLOS**, a sign language generation framework with temporally aligned gloss-level conditioning. First, we employ gloss-level conditions, which we define as sequences of gloss embeddings temporally aligned with the motion sequence. This enables the model to access both the temporal structure of sign language and word-level semantics at each timestep. As a result, this allows for fine-grained control of signs and better preservation of lexical order. Second, we introduce a condition fusion module, temporal alignment conditioning (TAC), to efficiently deliver the word-level semantic and temporal structure provided by the gloss-level condition to the corresponding motion timesteps. Our method, which is composed of gloss-level conditions and TAC, generates signs with correct lexical order and high semantic accuracy, outperforming prior methods on CSL-Daily and Phoenix-2014T.

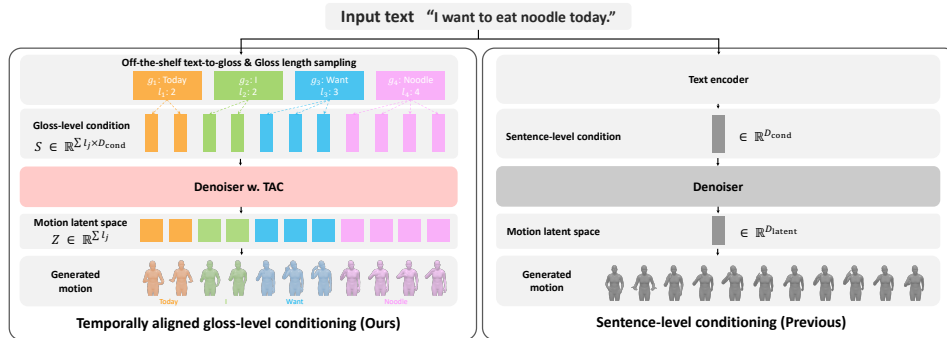


Figure 2: **Conceptual comparison.** We compare our temporally aligned gloss-level conditioning against conventional sentence-level conditioning. Our method leverages gloss-level conditions with temporal alignment conditioning (TAC) to ensure temporal alignment between gloss conditions and associated motion segments, generating signs in correct lexical order and high semantic accuracy.

1 Introduction

Sign language serves as a vital means of communication for millions of deaf and hard-of-hearing (DHH) individuals worldwide. Yet, communication between signers and non-signers remains limited, relying on the assistance of expert interpreters. As a key step toward lowering this communication barrier, text-to-sign generation (sign language generation, SLG [42, 3, 43, 37]) has recently begun to receive growing research attention. SLG plays an essential role in enabling automated subtitles and virtual assistants across media and public services.

Sign language conveys meaning through a sequence of gestures, each corresponding to a word-like linguistic unit known as a *gloss*. Each gloss-aligned gesture segment, referred to as a *lexical sign*, must follow the correct *lexical order* [25, 8] to ensure that the intended meaning is accurately delivered. As shown in Figure 1, previous approaches often suffer from incorrect lexical order and low semantic accuracy. A key reason lies in the use of sentence-level condition, where the entire input sentence is encoded into a single feature vector without considering the temporally sequential structure of sign language (see Figure 2, right). This strategy introduces two major limitations. First, the sentence-level condition fails to capture the temporal structure of sign language. Lacking explicit temporal structure, the model often produces signs with the wrong lexical order. Second, it lacks the granularity to convey fine-grained context at each timestep. This results in ambiguous gestures that do not clearly correspond to individual glosses. Together, these limitations hinder the ability to maintain both the lexical order and semantic accuracy essential for accurate sign language generation.

To address the above two limitations, we present **GLOS**, a sign language generation method with temporally aligned gloss-level conditioning. As shown in Figure 2 (left), our framework consists of two components: (1) gloss-level condition and (2) temporal alignment conditioning (TAC). First, we employ gloss-level conditions, defined as 2D sequences (temporal and channel dimensions) of gloss embeddings temporally aligned with the motion sequence. The gloss-level conditions capture both the sequential structure of sign language and the fine-grained semantics required at each timestep, thus overcoming the limitations of sentence-level condition. Notably, tokenized sequence of spoken language fails to reflect the temporal structure of sign language due to the difference in linguistic order. We instead extract glosses from the input text using an off-the-shelf text-to-gloss model [7] and temporally align the gloss embeddings with the motion sequence.

Second, we introduce TAC, a condition fusion module that integrates gloss-level conditions into the motion latent space over a local temporal range corresponding to each gloss and its surrounding timesteps. SLG aims to produce a structured sequence of motion frames from a sequence of glosses, and thus falls under the general class of sequence-to-sequence tasks. While Transformer-based cross-attention [34] is widely used in sequence-to-sequence tasks such as machine translation, we found it suboptimal for sign language generation. In cross-attention, each motion timestep globally attends to all gloss tokens, leading to excessive information mixing across time. In contrast, our TAC effectively delivers the word-level semantics provided by the gloss-level condition into the motion latent space at their corresponding timesteps and their temporally local neighborhood. We leverage

Adaptive Layer Normalization (AdaLN) [14] for temporal alignment-aware modulation, and 1D convolution to incorporate with local context. This alignment-aware design allows the model to better capture the sequential structure of sign language and generate more accurate, temporally coherent sign sequences.

Extensive experiments demonstrate that our approach substantially outperforms existing SLG methods on CSL-Daily [41] and Phoenix-2014T [4]. Our key contributions are summarized as follows.

- We propose GLOS, a sign language generation framework that leverages temporally aligned gloss-level conditioning.
- We introduce gloss-level conditions that deliver fine-grained, semantic information at each timestep, addressing the limitations of sentence-level conditioning.
- We design temporal alignment conditioning (TAC) to preserve temporal alignment between gloss conditions and motion timesteps, enabling accurate and temporally coherent sign generation.

2 Related works

Sign language generation Sign language generation (SLG) [3, 30, 29, 15, 43, 42, 38, 37] aims to synthesize accurate sign gesture sequences from text inputs, enabling machine-mediated communication with deaf and hard-of-hearing individuals. NSA [3] constructs a 3D sign language dataset and leverages it to train the diffusion model. SOKE [42] adapts a pretrained language model to generate sign language, employing a multi-head decoding strategy to efficiently fuse different body parts. T2S-GPT [37] proposes a GPT-based autoregressive generation framework based on the VAE-encoded discrete latent space. Spoken2Sign [43] presents a practical pipeline that extracts glosses from input texts, retrieves 3D signs corresponding to the glosses, and connects them to generate sign language.

Despite the notable progress in SLG, relatively little attention has been paid to the effective conditioning strategies for textual inputs. Most existing methods encode the input text as a sentence-level condition, which fails to capture the temporal structure of sign language and lacks the granularity to convey fine-grained context. Spoken2Sign [43] partially addresses this by incorporating gloss-level temporal alignment, but it does so by retrieving pre-defined sign gestures for each gloss independently and interpolating them. This often results in unrealistic transitions and overlooks the temporal dependencies between adjacent glosses. In contrast, our proposed GLOS models gloss-level conditions in an end-to-end generation framework, ensuring temporal alignment and local contextual integration. Unlike retrieval-based methods such as Spoken2Sign, our approach learns smooth transitions and captures dependencies between adjacent glosses via diffusion-based decoding [10].

Human motion generation Human motion generation [32, 6, 39, 17, 18, 16, 12, 27, 1, 19, 31, 11, 28, 40, 35] targets realistic and temporally coherent synthesis of body movements from text descriptions. ACTOR [27] learns action-conditioned motion embeddings using a Transformer-based VAE for diverse human motion generation. MDM [32] applies a denoising diffusion model in motion space to generate high-quality human motion from natural language descriptions. MotionGPT [16] treats human motion as a discrete token sequence and pre-trains a unified transformer across captioning and language understanding tasks. MoMask [12] introduces a hierarchical VQ framework with masked modeling to enhance fine-grained motion generation. While existing human motion generation methods can be adapted for sign language generation, naive adaptation results in temporal misalignment with gloss sequences. Our proposed TAC design enhances temporal alignment between glosses and generated motions to address this, enabling more accurate and expressive sign language synthesis. Further discussion is provided in Section 5.3.

3 Preliminary

3.1 VQ-VAE

VQ-VAE [33, 39] comprises an encoder E , a decoder G , and a codebook $\mathcal{Z} = \{\mathbf{z}_k \in \mathbb{R}^d\}_{k=1}^K$, where K is the number of codebook entries and d is the dimensionality of each code vector. Given an input motion $\mathbf{X} \in \mathbb{R}^{L \times D}$, where L and D denote the sequence length and feature dimension, respectively, the encoder maps it to a latent representation $\mathbf{Z}^e = E(\mathbf{X}) \in \mathbb{R}^{L' \times d}$. The length of the latent sequence

is defined as $L' = \lfloor L/r \rfloor$, where r denotes the temporal reduction rate of the encoder E . We denote the encoder outputs and quantized latent representation as \mathbf{Z}^e and \mathbf{Z}^q , respectively. Each latent vector \mathbf{Z}_i^e at temporal step i is quantized to the nearest codebook vector \mathbf{z}_k :

$$\mathbf{Z}_i^q = \mathbf{z}_k, \quad \text{where } k = \arg \min_{k'} \|\mathbf{Z}_i^e - \mathbf{z}_{k'}\|_2. \quad (1)$$

The decoder reconstructs the motion from the quantized latent codes $\hat{\mathbf{X}} = G(\mathbf{Z}^q)$. The VQ-VAE is trained to minimize the following loss function:

$$L = \|\mathbf{X} - \hat{\mathbf{X}}\|_2^2 + \|\text{sg}(\mathbf{Z}^e) - \mathbf{Z}^q\|_2^2 + \beta \|\mathbf{Z}^e - \text{sg}(\mathbf{Z}^q)\|_2^2, \quad (2)$$

where $\text{sg}(\cdot)$ is the stop-gradient operation, and β is a loss weight.

3.2 VQ-Diffusion

VQ-Diffusion [10] operates over discrete VQ tokens, a finite set of codebook indices, obtained from a pre-trained VQ-VAE. Unlike continuous diffusion models [13], which add Gaussian noise to real-valued inputs, this approach defines a discrete Markov diffusion process over VQ tokens.

Forward process. Let $\mathbf{k}_0 \in \{1, \dots, K\}^{L'}$ denote the original sequence of VQ tokens from the codebook. The forward diffusion process gradually corrupts \mathbf{k}_0 over T timesteps by randomly replacing tokens, defined by a transition matrix Q_t :

$$q(\mathbf{k}_t | \mathbf{k}_{t-1}) = \mathbf{v}^\top(\mathbf{k}_t) Q_t \mathbf{v}(\mathbf{k}_{t-1}), \quad (3)$$

where $\mathbf{v}(\cdot)$ denotes the one-hot representation of a VQ token, and $Q_t \in \mathbb{R}^{K \times K}$ is a stochastic matrix with rows summing to 1. The transition matrix is constructed using hyperparameters α_t , β_t , and γ_t , which control the probabilities of token retention, replacement with random tokens, and masking, respectively. At the final timestep T , all tokens are fully masked, and the masked sequence serves as the starting point for the reverse denoising process, analogous to sampling from a standard Gaussian distribution in continuous DDPM frameworks.

Reverse process. The goal of the reverse process is to recover \mathbf{k}_0 from a noisy \mathbf{k}_t . This is achieved by estimating the reverse transition:

$$p_\theta(\mathbf{k}_{t-1} | \mathbf{k}_t, \mathbf{y}) = \sum_{\tilde{\mathbf{k}}_0} q(\mathbf{k}_{t-1} | \mathbf{k}_t, \tilde{\mathbf{k}}_0) p_\theta(\tilde{\mathbf{k}}_0 | \mathbf{k}_t, \mathbf{y}), \quad (4)$$

where $\tilde{\mathbf{k}}_0$ is the predicted denoised VQ token sequence, and \mathbf{y} is a conditional input (e.g., text prompt). The denoiser model, which can be designed for the specific purpose such as sign language generation, predicts the initial state $p_\theta(\tilde{\mathbf{k}}_0 | \mathbf{k}_t, \mathbf{y})$. Denoiser is trained to estimate the posterior transition distribution $q(\mathbf{k}_{t-1} | \mathbf{x}_t, \mathbf{k}_0)$ with the variational lower bound [10].

4 GLOS

In this section, we describe our GLOS, which consists of gloss-level condition and temporal alignment conditioning (TAC) as illustrated in Figure 3. Our method adopts a body-part aware generative model based on VQ-Diffusion [10]. Section 4.1 details the body part-aware motion latent space learning using the PVQ-VAE. Section 4.2 presents the encoding of gloss-level conditions. Section 4.3 describes the details of VQ-diffusion generation, including the architecture of the denoiser with TAC.

4.1 Motion latent space learning via PVQ-VAE

Figure 3 left shows our motion latent space learning with the proposed PVQ-VAE. We learn the motion latent space using PVQ-VAE to enhance the expressiveness of hand and face, inspired by prior works [42, 5, 23]. Following the notations in Section 3.1, each input motion sequence \mathbf{X} is decomposed into \mathbf{X}^{body} , $\mathbf{X}^{\text{lhand}}$, $\mathbf{X}^{\text{rhand}}$, and \mathbf{X}^{face} . We denote the input motion sequence of each part by \mathbf{X}^{part} , where $\text{part} \in \{\text{body}, \text{lhand}, \text{rhand}, \text{face}\}$.

The input motion sequence of each part \mathbf{X}^{part} is processed by a dedicated 1D convolutional encoder E^{part} and decoder G^{part} , with a corresponding codebook of each part $\mathcal{Z}^{\text{part}} = \{\mathbf{z}_k^{\text{part}} \in \mathbb{R}^d\}_{k=1}^K$. Each

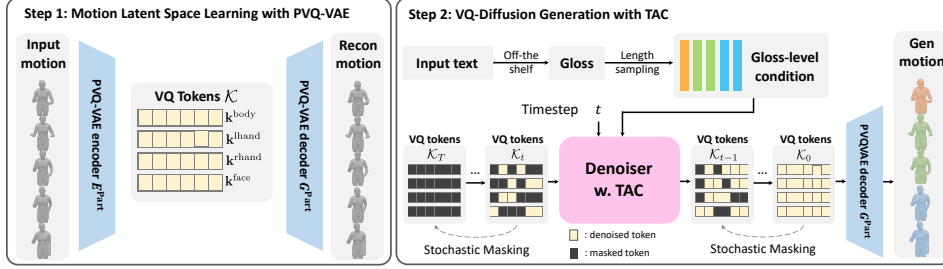


Figure 3: **Overview.** We first construct the motion latent space with PVQ-VAE (left). In generation phase (right), we first encode input text into gloss-level condition with off-the-shelf text-to-gloss model [7] and length sampling. Our proposed denoiser with TAC generates the tokens in the motion latent space and forwards them into the PVQ-VAE decoder to generate sign language.

input \mathbf{X}^{part} is encoded as $\mathbf{Z}^{e,\text{part}} = E^{\text{part}}(\mathbf{X}^{\text{part}})$, then quantized using the codebook into $\mathbf{Z}^{q,\text{part}}$. The quantized feature is decoded as $\hat{\mathbf{X}}^{\text{part}} = G^{\text{part}}(\mathbf{Z}^{q,\text{part}})$. Here, $\mathbf{Z}^{e,\text{part}}$ and $\mathbf{Z}^{q,\text{part}}$ denote the encoder output and the quantized latent of each part, respectively. The training objective minimizes the loss across all parts, $L = L^{\text{body}} + L^{\text{lhand}} + L^{\text{rhand}} + L^{\text{face}}$, with each term defined in Equation 2.

4.2 Gloss-level condition

As illustrated in Figure 3 (right top), we first convert the input text into a gloss sequence $g = \{g_j\}_j$ using an off-the-shelf text-to-gloss method [7]. We sample the mean length l_j for each gloss g_j from the training set to construct a length sequence $l = \{l_j\}_j$, where j represents gloss indices. For the glosses which are not included in the training set, we utilize the mean length of all glosses.

We extract the text embedding of gloss $c_j \in \mathbb{R}^{D_{\text{cond}}}$ for each g_j using pre-trained mBART [22], where D_{cond} denotes the channel dimension of the condition vector. Then, as shown in the second row in Figure 2 left, we repeat each gloss feature c_j for l_j steps and stack them sequentially to obtain the gloss-level condition $S \in \mathbb{R}^{L \times D_{\text{cond}}}$. Note that $L = \sum_j l_j$ denotes the total desired motion length. The resulting gloss-level condition provides both the sequential structure of sign language and word-level semantics at each timestep, enabling accurate and temporally ordered sign generation.

4.3 VQ-diffusion generation with temporal alignment conditioning (TAC)

In this section, we describe the VQ-Diffusion generation process with TAC. First, we describe the architecture of the denoiser. Then, we present TAC to promote temporal alignment during condition fusion. We also introduce inter-part attention (IPA) to enable coordinated movements across articulators, which is critical when separately encoding the body part with PVQ-VAE.

Architecture. Figure 4a visualizes the architecture of the proposed denoiser. Each body part—body, left hand, right hand, and face—is forwarded independently without inter-part interaction, except within the IPA module. To be specific, for each part, we first represent VQ tokens $\mathbf{k}^{\text{part}} \in \mathbb{R}^L$ as a vector of codebook indices. The VQ tokens are formed into embedded tokens $\mathbf{X}_{\text{embed}}^{\text{part}} \in \mathbb{R}^{L \times D_{\text{feat}}}$. D_{feat} denotes the channel dimension of the feature, and is maintained throughout the denoiser forward pass. Then, we integrate the diffusion timestep t into the embedded tokens $\mathbf{X}_{\text{embed}}^{\text{part}}$ using adaptive layer normalization (AdaLN) [14], resulting in $\mathbf{X}_{\text{time}}^{\text{part}}$. This is passed through a self-attention (SA) layer followed by a residual connection, yielding $\mathbf{X}_{\text{SA}}^{\text{part}} = \text{SA}(\mathbf{X}_{\text{time}}^{\text{part}}) + \mathbf{X}_{\text{embed}}^{\text{part}}$. Next, $\mathbf{X}_{\text{SA}}^{\text{part}}$ is processed by the inter-part attention (IPA) module with a residual connection, producing $\mathbf{X}_{\text{IPA}}^{\text{part}} = \text{IPA}(\mathbf{X}_{\text{SA}}^{\text{part}}) + \mathbf{X}_{\text{SA}}^{\text{part}}$. Finally, the features are fused with the gloss-level condition S in TAC, resulting in the output $\mathbf{X}_{\text{TAC}}^{\text{part}}$.

Inter-part attention (IPA). Figure 4b illustrates the architecture of our proposed IPA module. It is designed to enhance the denoising process by enabling coordinated movements across articulators through inter-part feature integration. IPA operates on the features of the body, left hand, and right hand. Each of these features is first normalized with LayerNorm [2] and then used as a query in cross-attention with other body parts. Specifically, the body features attend to a concatenation of the hand features, while each hand attends to the body features. The model captures dependencies

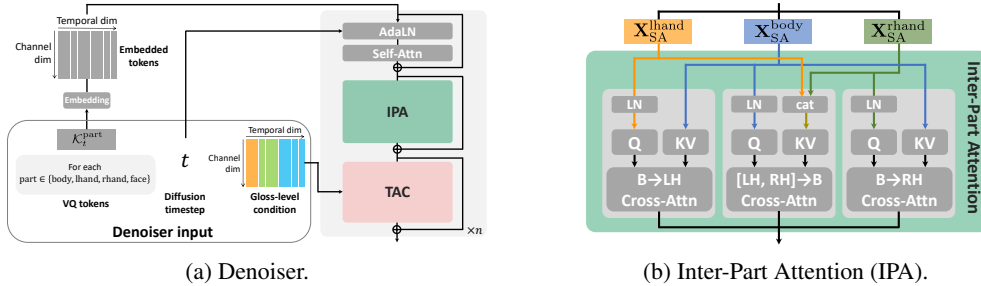


Figure 4: **Model architecture.** We illustrate the detailed architecture of our proposed denoiser and inter-part attention (IPA) module. (a) In our model, each body part—body, left hand, right hand, and face—is encoded independently without inter-part interaction, except within the IPA module. (b) Cross-attention between different body parts in the IPA block facilitates more coordinated movements of articulations, leading to a better quality of generated sign language.

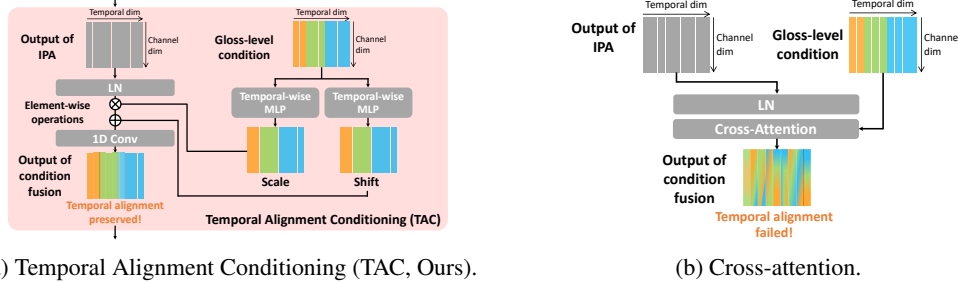


Figure 5: **Comparison of condition fusion methods.** We visualize two condition fusion methods: (a) Our TAC consists of AdaLN and 1D convolution to preserve the temporal alignment with local temporal context. (b) Cross-attention, which fails to maintain the temporal alignment constraint.

between body parts through this cross-attention mechanism, producing refined features for the body and both hands. We do not apply IPA to the face branch, as it did not improve our experiments.

Temporal alignment conditioning (TAC). Figure 5a shows the proposed TAC for condition fusion, consisting of AdaLN and a temporal 1D convolution. TAC effectively delivers each gloss-level semantics into the motion latent space over a local temporal range to the corresponding timestep of each gloss and its surrounding timesteps. This enables the model to capture the sequential structure of sign language, ensuring both precise alignment and semantic accuracy.

Given a gloss-level condition $S \in \mathbb{R}^{L \times D_{\text{feat}}}$, two temporal-wise MLPs independently produce scale $u \in \mathbb{R}^{D_{\text{feat}}}$ and shift $v \in \mathbb{R}^{D_{\text{feat}}}$. These vectors are used to modulate the input features via AdaLN, followed by a 1D convolution. The overall operation is defined as $\mathbf{X}_{\text{TAC}}^{\text{part}} = \text{Conv1D}(\text{LN}(\mathbf{X}_{\text{IPA}}^{\text{part}}) \otimes (1 + u) \oplus v)$, where \otimes and \oplus denote element-wise multiplication and addition, respectively. Through this design, AdaLN ensures that each gloss condition is aligned to its corresponding timestep, while the 1D convolution allows the model to consider local context for stable and coherent generation. Ablation study proves that our alignment-aware fusion strategy outperforms the cross-attention, allowing each motion timestep to attend all gloss tokens (Figure 5b).

5 Experiment

5.1 Protocols

Datasets. We use two large-scale sign language datasets: CSL-Daily [41] and PHOENIX-2014T [4], which contain approximately 20K and 8K samples, respectively, in Chinese and German sign languages. Our experiments are evaluated with a maximum sign length of 180 frames [32, 39].

Evaluation metrics. Following prior work [42, 3, 43], we evaluate the quality of the generated sign using multiple metrics targeting motion accuracy and linguistic fidelity. For motion-level evaluation, we use dynamic time warping with joint position error (DTW-JPE)[24], which measures the distance between aligned joint trajectories of generated and reference motions. To evaluate linguistic fidelity,

Table 1: **Effectiveness of gloss-level condition and TAC.** We validate the contribution of gloss-level condition and TAC with comparing different combinations of feature types, and conditioning methods. Our method appears in the last row.

Features	Temporal dim	Condition fusion	DTW-JPE↓			Back translation		
			Body	Hand	All	WER↓	BLEU-4↑	ROUGE↑
Text	✗	AdaLN + 1D Conv (TAC)	0.242	0.579	0.411	93.53	1.89	14.70
Gloss	✗	AdaLN + 1D Conv (TAC)	0.275	0.722	0.447	98.24	0.45	10.99
Gloss	✓	Cross Attention	0.247	0.584	0.416	96.66	0.57	11.65
Gloss	✓	AdaLN + FC	0.212	0.492	0.364	77.87	7.47	25.78
Gloss	✓	AdaLN + 1D Conv (TAC, Ours)	0.201	0.443	0.347	62.24	13.27	35.83

Table 2: **Effectiveness of IPA.** We validate the contribution of IPA by testing various combinations of attention flows: Body→Hands (B→H), Hands→Body (H→B), and Body→Face (B→F). Our method appears in the last row.

Attention			DTW-JPE↓			Back translation		
B→H	H→B	B→F	Body	Hand	All	WER↓	BLEU-4↑	ROUGE↑
✗	✗	✗	0.207	0.451	0.356	70.11	10.33	31.99
✓	✗	✗	0.203	0.451	0.352	63.06	11.77	34.71
✗	✓	✗	0.206	0.464	0.353	69.37	10.67	32.11
✓	✗	✓	0.202	0.452	0.350	62.55	12.30	35.00
✗	✓	✓	0.202	0.453	0.348	63.91	12.48	35.31
✓	✓	✓	0.203	0.452	0.347	62.67	12.79	35.48
✓	✓	✗	0.201	0.443	0.347	62.24	13.27	35.83

we adopt a back-translation approach using a continuous sign language recognition (CSLR) model [7], which maps generated signs back to gloss or text. Since the CSLR model [7] was unable to reproduce in our system due to the limited resources, we re-implemented a compatible feature encoder. We report word error rate (WER)[21] for sign-to-gloss evaluation, reflecting the edit distance between predicted and reference glosses. For sign-to-text evaluation, we use BLEU-4[26] and ROUGE [20], which compute n-gram precision and recall, respectively. Both metrics are sensitive to word order, making them suitable for evaluating the lexical order of generated signs.

Baselines. Since the evaluation system for previous methods was not publicly available [3, 42] or not reproducible due to the limit of the computational resource [43, 7], we could not reuse previously reported quantitative results to compare with ours. Instead, we re-ran experiments on CSL-Daily and PHOENIX-2014T using official implementations where available [16, 32, 12], or reproduced the baselines [37, 3, 42] ourselves when code was not publicly released.

5.2 Ablation Study

In this section, we present the ablation study to validate our contributions. We use lengths from the test set sample for ablation studies for the gloss-aligned condition, TAC and IPA to ensure a controlled experimental setting. For robustness analysis, we instead sample from the training set to evaluate robustness thoroughly.

Gloss-aligned condition and Temporal alignment conditioning (TAC). Table 1 clearly demonstrates the effectiveness of our method, which combines gloss-level condition and TAC. We first observe that sentence-level conditions without temporal structure lead to poor performance (first row). Similarly, 1D gloss embeddings encoded similarly as sentence-level conditions (visualized in the top-right of Figure 2) also result in low performance (second row). Even with gloss-level conditions, applying cross-attention without preserving temporal alignment (third row) fails to improve performance, highlighting the importance of temporal alignment. This is because, unlike our TAC module, which integrates the gloss condition over a corresponding local temporal range in the motion space, cross-attention allows each motion timestep to attend to all gloss tokens. Such global integration disrupts the temporal alignment between glosses and motion, leading to excessive mixing of information across time. Finally, comparing AdaLN with a fully-connected layer (fourth row) to our TAC block confirms that incorporating local context via 1D convolution brings substantial performance gains. The fully-connected layer is applied independently at each time step, without leveraging local context from neighboring time steps. These results suggest that the performance gain stems from providing temporal structure and fine-grained semantics of a sign through gloss-level conditions and preserving temporal alignment through TAC.

Table 3: **Robustness of our system.** We show the robustness of our method on the choice of text-to-gloss models and the variation of input length. Our method appears in the last row.

(a) Robustness to text-to-gloss models.							(b) Robustness to input length variation.						
Text-to-gloss method	DTW-JPE↓			Back translation			Length variation	DTW-JPE↓			Back translation		
	Body	Hand	All	WER↓	B-4↑	ROUGE↑		Body	Hand	All	WER↓	B-4↑	ROUGE↑
mT5 finetuned	0.238	0.536	0.422	73.84	16.74	41.76	length + 8	0.229	0.479	0.420	58.12	14.13	38.08
M2M finetuned	0.231	0.526	0.401	70.19	16.15	41.60	length + 4	0.222	0.477	0.401	55.47	16.40	40.89
mBART finetuned	0.229	0.523	0.395	70.17	17.21	41.42	length - 4	0.208	0.468	0.365	56.88	14.91	38.62
Off-the-shelf [7]	0.214	0.467	0.377	55.15	15.70	40.43	length + 0	0.214	0.467	0.377	55.15	15.70	40.43

Table 4: **Comparison to state-of-the-art methods.** We report the qualitative comparison with previous state-of-the-art methods on the CSL-Daily and Phoenix-2014T datasets. Our GLOS outperforms previous methods by a large margin on both datasets, regardless of the input length sampled from the training or test set.

Method	CSL-Daily						Phoenix-2014T					
	DTW-JPE↓			Back translation			DTW-JPE↓			Back translation		
	Body	Hand	All	WER↓	BLEU-4↑	ROUGE↑	Body	Hand	All	WER↓	BLEU-4↑	ROUGE↑
T2S-GPT [37]	0.278	0.644	0.453	93.01	2.05	16.57	0.593	1.037	0.825	98.40	2.35	8.78
MotionGPT [16]	0.653	0.901	0.797	95.04	2.08	15.63	0.907	1.145	1.024	94.08	5.54	15.51
MDM [32]	0.318	0.748	0.529	95.54	3.01	17.29	0.427	1.061	0.748	98.27	5.44	14.90
MoMask [12]	0.314	0.641	0.492	91.36	3.57	19.77	0.355	0.675	0.538	91.33	6.92	21.77
NSA [3]	0.314	0.740	0.523	95.40	1.72	15.18	0.309	0.680	0.541	94.18	6.24	18.73
SOKE [42]	0.272	0.649	0.447	95.68	1.95	15.62	0.258	0.589	0.441	97.84	4.23	13.16
Ours (Test len)	0.201	0.443	0.347	62.24	13.27	35.83	0.222	0.520	0.381	87.93	8.54	24.38
Ours (Train len)	0.214	0.467	0.377	55.15	15.70	40.43	0.228	0.524	0.400	84.44	8.28	22.95

Inter-part attention (IPA). Table 2 shows that IPA improves sign language generation performance notably. We refer the body-to-hands ($B \rightarrow H$) to the left and right branches of the Figure 4b, and hands-to-body ($H \rightarrow B$) attention to the branch in the center. The body-to-face ($B \rightarrow F$) attention is not illustrated in the figure, since it is not included in our final IPA design. Individually applying $B \rightarrow H$ and $H \rightarrow B$ attentions (second and third rows) yield performance gain over the baseline without IPA (first row). Adding $B \rightarrow F$ attention offers additional improvements (fourth and fifth rows). However, when both $B \rightarrow H$ and $H \rightarrow B$ attentions are already active (last row), adding $B \rightarrow F$ (sixth row) slightly degrades performance. We attribute this to the limited diversity of facial expressions in the training set, making face features less informative and potentially introducing redundant or noisy signals beyond the already rich body-hand interactions. Based on these findings, we adopt the cross-attention between body and hands as our final IPA design, as illustrated in Figure 4b.

Robustness on text-to-gloss and length sampling. Table 3 demonstrates the robustness of our method against variations in both text-to-gloss models and sign lengths. The left block reports the quantitative results using baseline text-to-gloss methods based on fine-tuned mT5 [36], M2M [9], and mBART [22]. While there is a slight degradation in DTW-JPE and WER, our model consistently achieves strong back-translation accuracy, indicating robustness to different text-to-gloss methods. The right block evaluates performance under varying sign lengths. Here, input lengths were perturbed within a range of -4 to $+8$ relative to the original. Given that the average lexical sign length in CSL-Daily is 16, this corresponds to approximately -25% to $+50\%$ variation. Our model maintains stable performance across this range, demonstrating strong temporal robustness.

5.3 Comparison to state-of-the-art methods

Table 4 clearly demonstrates that our proposed GLOS substantially outperforms previous methods on both the CSL-Daily [41] and Phoenix-2014T [4] datasets. We report results under two sign length sampling strategies: using the length from test set samples (seventh row) and sampling from the training set (last row). In both settings, GLOS consistently outperforms all baselines.

On CSL-Daily (left block), GLOS achieves significant improvements over existing methods. While MoMask [12] reports the best back-translation score among prior works, and SOKE [42] yields the best DTW-JPE scores, our method surpasses all of them by a clear margin across both metrics. Similarly, on Phoenix-2014T (right block), GLOS also achieves state-of-the-art results. Although MoMask and SOKE show strong performance in back-translation and DTW-JPE, respectively, our method consistently outperforms their best results, regardless of the sampling strategy.

Figure 6 shows that our GLOS generates accurate sign language in correct lexical order compared with MoMask [12] and NSA [3], which show the best performance among previous methods. Each

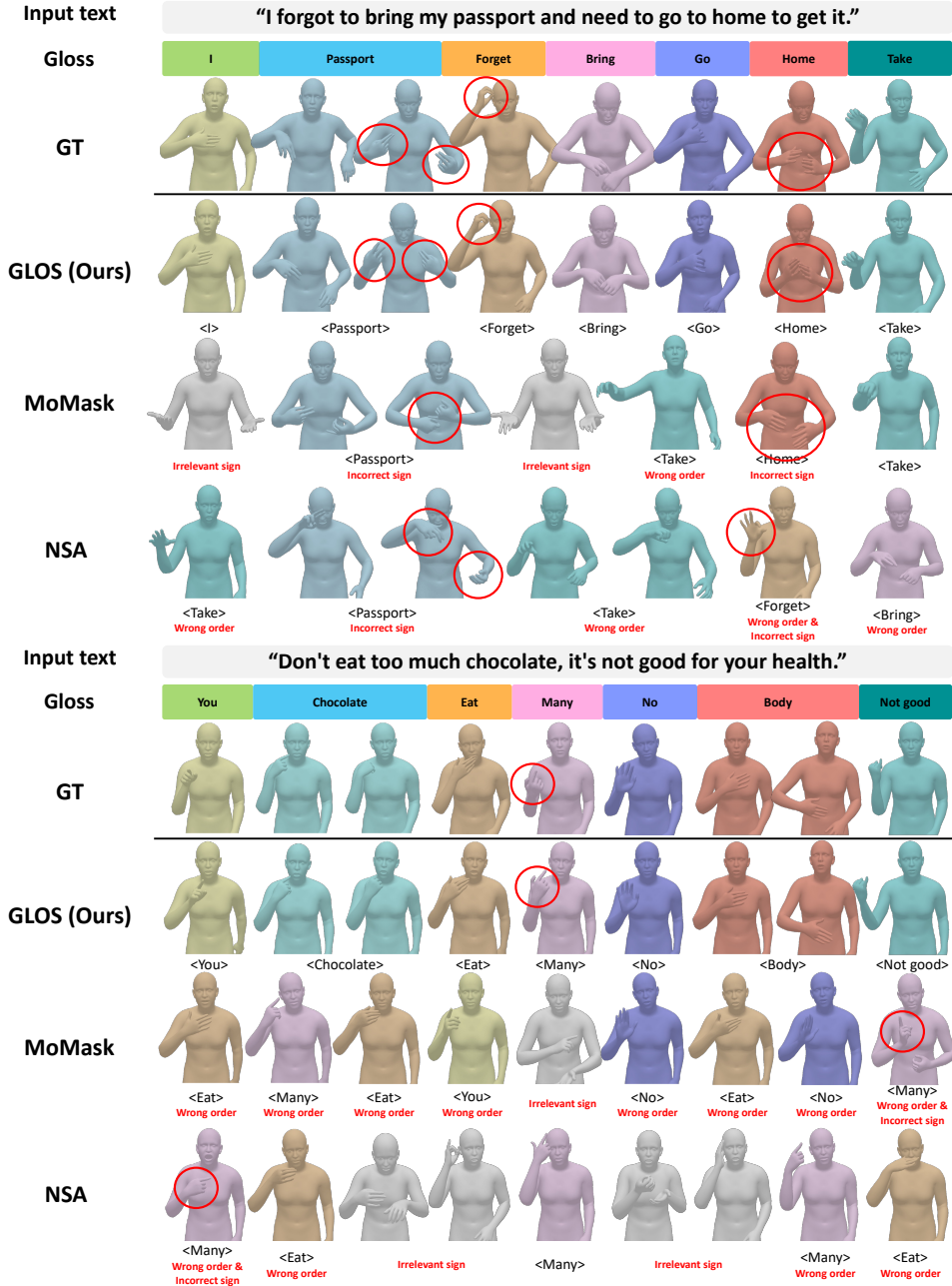


Figure 6: **Qualitative result.** We present the qualitative comparison of our GLOS with GT, MoMask [12], and NSA [3].

gloss is represented by their own colors, and the corresponding lexical signs are also represented in the same colors as the glosses. Human-interpreted glosses are denoted inside brackets < >.

6 Conclusion

We proposed GLOS, a sign language generation framework with temporally aligned gloss-level conditioning. By incorporating gloss-level conditions and TAC, GLOS addresses key limitations of sentence-level conditioning: the lack of temporal structure of sign language and lack of granularity to convey fine-grained context of each timestep. By overcoming two limitations above, our GLOS successfully generates accurate sign language. Our proposed method highly outperforms previous methods on CSL-Daily and Phoenix-2014T datasets.

References

- [1] Nikos Athanasiou, Mathis Petrovich, Michael J. Black, and Gül Varol. TEACH: Temporal Action Compositions for 3D Humans. In *3DV*, 2022.
- [2] Jimmy Lei Ba, Jamie Ryan Kiros, and Geoffrey E Hinton. Layer normalization. In *arXiv*, 2016.
- [3] Vasileios Baltatzis, Rolandos Alexandros Potamias, Evangelos Ververas, Guanxiong Sun, Jiankang Deng, and Stefanos Zafeiriou. Neural Sign Actors: A diffusion model for 3d sign language production from text. In *CVPR*, 2024.
- [4] Necati Cihan Camgoz, Simon Hadfield, Oscar Koller, Hermann Ney, and Richard Bowden. Neural sign language translation. In *CVPR*, 2018.
- [5] Changan Chen, Juze Zhang, Shrinidhi Kowshika Lakshmikanth, Yusu Fang, Ruizhi Shao, Gordon Wetzstein, Li Fei-Fei, and Ehsan Adeli. The language of motion: Unifying verbal and non-verbal language of 3d human motion. In *arXiv*, 2024.
- [6] Xin Chen, Biao Jiang, Wen Liu, Zilong Huang, Bin Fu, Tao Chen, and Gang Yu. Executing your commands via motion diffusion in latent space. In *CVPR*, 2023.
- [7] Yutong Chen, Ronglai Zuo, Fangyun Wei, Yu Wu, Shujie Liu, and Brian Mak. Two-stream network for sign language recognition and translation. In *NeurIPS*, 2022.
- [8] Qi Cheng and Rachel I Mayberry. Acquiring a first language in adolescence: The case of basic word order in american sign language. *Journal of child language*, 46(2):214–240, 2019.
- [9] Angela Fan, Shruti Bhosale, Holger Schwenk, Zhiyi Ma, Ahmed El-Kishky, Siddharth Goyal, Mandeep Baines, Onur Celebi, Guillaume Wenzek, Vishrav Chaudhary, Naman Goyal, Tom Birch, Vitaliy Liptchinsky, Sergey Edunov, Edouard Grave, Michael Auli, and Armand Joulin. Beyond english-centric multilingual machine translation. In *arXiv*, 2020.
- [10] Shuyang Gu, Dong Chen, Jianmin Bao, Fang Wen, Bo Zhang, Dongdong Chen, Lu Yuan, and Baining Guo. Vector quantized diffusion model for text-to-image synthesis. In *CVPR*, 2022.
- [11] Chuan Guo, Xinxin Zuo, Sen Wang, and Li Cheng. TM2T: Stochastic and tokenized modeling for the reciprocal generation of 3d human motions and texts. In *ECCV*, 2022.
- [12] Chuan Guo, Yuxuan Mu, Muhammad Gohar Javed, Sen Wang, and Li Cheng. MoMask: Generative masked modeling of 3d human motions. In *CVPR*, 2024.
- [13] Jonathan Ho, Ajay Jain, and Pieter Abbeel. Denoising diffusion probabilistic models. In *NeurIPS*, 2020.
- [14] Xun Huang and Serge Belongie. Arbitrary style transfer in real-time with adaptive instance normalization. In *ICCV*, 2017.
- [15] Eui Jun Hwang, Jung Ho Kim, Suk Min Cho, and Jong C. Park. Non-autoregressive sign language production via knowledge distillation. In *BMVC*, 2021.
- [16] Biao Jiang, Xin Chen, Wen Liu, Jingyi Yu, Gang Yu, and Tao Chen. MotionGPT: Human motion as a foreign language. In *NeurIPS*, 2024.
- [17] Taeryung Lee, Gyeongsik Moon, and Kyoung Mu Lee. MultiAct: Long-term 3d human motion generation from multiple action labels. In *AAAI*, 2023.
- [18] Taeryung Lee, Fabien Baradel, Thomas Lucas, Kyoung Mu Lee, and Gregory Rogez. T2LM: Long-term 3d human motion generation from multiple sentences. In *CVPR Workshop on Human Motion Generation*, 2024.
- [19] Shuai Li, Sisi Zhuang, Wenfeng Song, Xinyu Zhang, Hejia Chen, and Aimin Hao. Sequential texts driven cohesive motions synthesis with natural transitions. In *ICCV*, 2023.
- [20] Chin-Yew Lin. Rouge: A package for automatic evaluation of summaries. In *Text summarization branches out*, 2004.

- [21] Chin-Yew Lin and Franz Josef Och. Automatic evaluation of machine translation quality using longest common subsequence and skip-bigram statistics. In *Proceedings of the 42nd annual meeting of the association for computational linguistics (ACL-04)*, pages 605–612, 2004.
- [22] Yinhan Liu, Jiatao Gu, Naman Goyal, Xian Li, Sergey Edunov, Marjan Ghazvininejad, Mike Lewis, and Luke Zettlemoyer. Multilingual denoising pre-training for neural machine translation. *Transactions of the Association for Computational Linguistics*, 8:726–742, 2020.
- [23] Shunlin Lu, Ling-Hao Chen, Ailing Zeng, Jing Lin, Ruimao Zhang, Lei Zhang, and Heung-Yeung Shum. Humantomato: Text-aligned whole-body motion generation. In *arXiv*, 2023.
- [24] Meinard Müller. *Information retrieval for music and motion*, volume 2. Springer, 2007.
- [25] Donna Jo Napoli and Rachel Sutton-Spence. Order of the major constituents in sign languages: Implications for all language. *Frontiers in psychology*, 5:376, 2014.
- [26] Kishore Papineni, Salim Roukos, Todd Ward, and Wei-Jing Zhu. Bleu: a method for automatic evaluation of machine translation. In *ACL*, 2002.
- [27] Mathis Petrovich, Michael J. Black, and Gül Varol. Action-conditioned 3D human motion synthesis with transformer VAE. In *ICCV*, 2021.
- [28] Mathis Petrovich, Michael J. Black, and Gül Varol. TEMOS: Generating diverse human motions from textual descriptions. In *ECCV*, 2022.
- [29] Ben Saunders, Necati Cihan Camgoz, and Richard Bowden. Adversarial training for multi-channel sign language production. In *BMVC*, 2020.
- [30] Ben Saunders, Necati Cihan Camgoz, and Richard Bowden. Progressive transformers for end-to-end sign language production. In *ECCV*, 2020.
- [31] Yoni Shafir, Guy Tevet, Roy Kapon, and Amit Haim Bermano. Human motion diffusion as a generative prior. In *ICLR*, 2024.
- [32] Guy Tevet, Sigal Raab, Brian Gordon, Yoni Shafir, Daniel Cohen-or, and Amit Haim Bermano. Human motion diffusion model. In *ICLR*, 2023.
- [33] Aaron Van Den Oord, Oriol Vinyals, et al. Neural discrete representation learning. In *NeurIPS*, 2017.
- [34] Ashish Vaswani, Noam Shazeer, Niki Parmar, Jakob Uszkoreit, Llion Jones, Aidan N Gomez, Łukasz Kaiser, and Illia Polosukhin. Attention is all you need. In *NeurIPS*, 2017.
- [35] Bizhu Wu, Jinheng Xie, Keming Shen, Zhe Kong, Jianfeng Ren, Ruibin Bai, Rong Qu, and Linlin Shen. Mg-motionllm: A unified framework for motion comprehension and generation across multiple granularities. In *CVPR*, 2025.
- [36] Linting Xue, Noah Constant, Adam Roberts, Mihir Kale, Rami Al-Rfou, Aditya Siddhant, Aditya Barua, and Colin Raffel. mT5: A massively multilingual pre-trained text-to-text transformer. In *NAACL*, 2021.
- [37] Aoxiong Yin, Haoyuan Li, Kai Shen, Siliang Tang, and Yueting Zhuang. T2S-GPT: Dynamic vector quantization for autoregressive sign language production from text. In *ACL*, 2024.
- [38] Zhengdi Yu, Shaoli Huang, Yongkang Cheng, and Tolga Birdal. SignAvatars: A large-scale 3d sign language holistic motion dataset and benchmark. In *ECCV*, 2024.
- [39] Jianrong Zhang, Yangsong Zhang, Xiaodong Cun, Shaoli Huang, Yong Zhang, Hongwei Zhao, Hongtao Lu, and Xi Shen. T2M-GPT: Generating human motion from textual descriptions with discrete representations. In *CVPR*, 2023.
- [40] Mingyuan Zhang, Zhongang Cai, Liang Pan, Fangzhou Hong, Xinying Guo, Lei Yang, and Ziwei Liu. MotionDiffuse: Text-driven human motion generation with diffusion model. *IEEE TPAMI*, 2024.

- [41] Hao Zhou, Wengang Zhou, Weizhen Qi, Junfu Pu, and Houqiang Li. Improving sign language translation with monolingual data by sign back-translation. In *CVPR*, 2021.
- [42] Ronglai Zuo, Rolandos Alexandros Potamias, Evangelos Ververas, Jiankang Deng, and Stefanos Zafeiriou. Signs as Tokens: A retrieval-enhanced multilingual sign language generator. In *arXiv*, 2024.
- [43] Ronglai Zuo, Fangyun Wei, Zenggui Chen, Brian Mak, Jiaolong Yang, and Xin Tong. A simple baseline for spoken language to sign language translation with 3d avatars. In *ECCV*, 2024.

NeurIPS Paper Checklist